Structural Performance of Ti6Al4V Tibial Tray in Total Knee Arthroplasty (TKA) by Functionally Graded Lattice Structures using Numerical Analysis

Nurasyrani Rabuan[1], Mohd Shahriman Adenan[1,2], Yupiter HP Manurung[1,2]*
Mohd Afzan Mohd Anuar[2], Solehuddin Shuib[2]

[1]Smart Manufacturing Research Institute, Universiti Teknologi MARA, Shah Alam, 40450, Selangor, MALAYSIA
[2]School of Mechanical Engineering, College of Engineering, Universiti Teknologi MARA, Shah Alam, 40450, Selangor, MALAYSIA
[*]mshahriman@uitm.edu.my

ABSTRACT

The medical industry benefits greatly from the additive manufacturing (AM) technology used on customized products. Total knee arthroplasty (TKA) has been widely used however it has drawbacks of stress shielding and loosening due to the excessive daily routine of patients. The problem could be minimized by applying lattice structures to the implant and mimicking the actual density of human bone. This study aims to investigate the optimal design of a Ti6Al4V alloy tibial tray by applying different types of lattice structure designs. A finite element analysis was used to investigate the mechanical behavior of uniform and non-uniform lattice structures in a walking position. Functional gradation structure was optimized on selected regions of the tibial tray with weight reduction and adaptation to the near actual density of the human bone without compromising its mechanical performance. The results indicated that the Voronoi structure has improved stress behavior and the capability to withstand the loads exerted, based on the Von Mises stress result of the Voronoi structure at 35.83 MPa as compared to the gyroid and diamond structures at 61.65 MPa and 49.74 MPa, respectively. The optimal design of the tibial implant was achieved by functionally graded lattice structures, replacing the solid tibial implant.

ISSN 1823-5514, eISSN 2550-164X

https://doi.org/10.24191/jmeche.v12i1.24643

Received for review: 2023-04-03
Accepted for publication: 2023-09-25
Published: 2023-11-15

Keywords: *Topology Optimization; TPMS Structures; Voronoi Structure; Finite Element Analysis; Tibial Tray*

Introduction

The rapid development of Additive Manufacturing (AM) technologies contributes towards the expansion of the industry's design and engineering approach. This technology is a process to manufacture solid parts through layer-by-layer addition of material by melting the material from a heat source [1]. Selective Laser Melting (SLM) is a process based on laser melted metal powder. This process also offers advantages in complex geometry, low manufacturing cost, and reduced fabrication time [2]. Furthermore, AM has been widely applied in biomedical industries, especially for orthopedics, implants, and human tissue.

In knee replacement surgery, artificial arthroplasty aims to relieve pain, improve function, and restore range of motion in the patients [3]. Anyhow, failures still occur after the replacement surgery such as loosening, wear, and stress shielding of the implant [4]-[5]. In a previous study, an assessment of the population was conducted to show the factors that affected the failure of tibial tray performance [6]. Another clinical study demonstrated a tibial plateau fracture caused by the patient's excessive weight [7].

To overcome the failure of implants, several studies proved that the combination of topology optimization by lattice structure and orthopedic implants has shown the enhancement of mechanical behaviour. Peto et al. [8] investigated the mechanical behaviour of Hexagonal Prism Vertex Centroid (HPVC) lattice structure which showed that lattice structures have an impact in reducing stiffness between implant and bones and minimizing stress shielding problems. Guoqing stated that due to excellent biocompatibility and good mechanical properties of the bio-fixation (solid and porous) implants, the life quality of patients has improved. The implants had been manufactured through the Selective laser melting (SLM) process [9]. Besides, this approach not only minimizes the implant weight but also facilitates tissue regeneration at the implant-bone interface. Triply Periodic Minimal Surfaces (TPMS) are common lattice structures used in the optimization of implants such as gyroid, diamond, and schwarz. There are two types of TPMS lattice structures which are solid-networks and sheet-networks types, whereas the properties for each type of lattice structure are also different [10]. Sheet-networks lattice structures show better mechanical properties compared to solid-networks lattice structures [11]. Yang et al. [12] proposed a gyroid unit cell (TPMS) made of Ti6Al4V, whose characteristic shows good strength and high manufacturability.

Yan et al. [13] developed gyroid and diamond TPMS lattices of bone implants with a percentage porosity of 80-95% for diamond and gyroid lattice

structures comparable to the porosity of trabecular bone which is 50-90%. As the value of porosity between implant and bone is almost similar, the modulus of porosity can be adjusted to the modulus of trabecular and cortical bone which may lead to reducing stress shielding problems. Lorenzo [14] compiled the reviews of AM-printed acetabular cups for total hip arthroplasty based on porous structure design, limitations of the manufacturing process, and clinical outcomes. The main highlight of the study was the comparison of conventional manufacturing such as die casting, CNC machining, and injection molding with AM printing and the enhancement of complex porous structures. Most recently, Limmahakun et al. [15] explored the optimization of orthopedic implants by functional gradation of lattice structures. The result showed that the mechanical strength gradually increased. According to Al-Ketan outcomes [16], these types of TPMS with sheet-network lattices encourage good mechanical behaviour, for example, could help improve tibial implant in structurally efficient, exhibiting better stiffness and strength to-weight ratio. In addition, the Voronoi structure showed that the irregularity of shape contributes to good mechanical behaviour which could attain stiffness comparable to bone stiffness [17]. Liang et al. [18] had proven trabecular-like porous structures with porosities between 48.83-74.28% had excellent mechanical performance in terms of elastic modulus and ultimate strength which is similar to cancellous bone mechanical behavior. Benedetti et al. [19] constructed a study of compressive behavior on nine different Ti6Al4V trabecular structures with various values of density, which displayed cross structure had the highest strength at constant stiffness compared to other structures.

The purpose of this research is to optimize the tibial tray of the TKA implant using a topology optimization approach by obtaining a suitable density compared to human bone and weight reduction. Advanced lattice structures have been proposed for optimizing the tibial component. The geometrical model of the tibial tray was first constructed, and then the Finite Element (FE) model was developed. The mechanical behaviour of the tibial tray was analysed using Finite Element Analysis (FEA). Specific regions of the tibial tray were replaced by three different lattice structures, namely, 1) gyroid, 2) diamond sheet structures, and 3) Voronoi strut structure due to stretching-dominated behavior which exhibited higher fracture strength compared to bending-dominated [21]. Their mechanical performance was analysed and evaluated by implementing similar boundary conditions and loadings. In order to improve further design and mechanical properties, functional gradation of lattice structure was applied during the optimization process.

Materials and Method

Model designs of total knee implant

Total knee replacement as shown in Figure 1 consists of three components: (a) femoral, (b) tibial insert, and (c) tibial. As for this research, it only focused on the mechanical behaviour of the tibial tray as stress shielding always occurs between the tibial tray and human bone due to a mismatch of stiffness. The tibial tray is available in a variety of complex geometric shapes and surfaces. Many factors need to be considered while designing an implant to ensure the implantation effectiveness which decreases the incidence of implant loosening. The tibial tray design for this investigation was derived from a previous study since the design has been established [20]. As indicated in Figure 2a, the tibial tray is a stem and the tibial wing to increase the stability of total knee replacement and reduce micromotion [21]. The tibial insert hole as in Figure 2b is functioning as a tibial insert holder. Figure 2c depicts the main geometric dimension of the designed tibial tray.

Lattice structure composition

This study uses the TPMS with gyroid and diamond sheet structures and Voronoi strut structures for the optimization phase due to its capability to withstand high stress loads and the most prominent structures with increased strength. The following equation shows the level-set equations of the TPMS gyroid (φ_G) and diamond (φ_D) geometries [23]-[25]:

$$\varphi_G = \sin x \cos y + \sin y \cos z + \sin z \cos x = c \quad (1)$$

$$\varphi_D = \cos x \cos y \cos z - \sin x \sin y \sin z = c \quad (2)$$

The FEA Voronoi structure is configured to resemble the bone trabecular structure, with structures created in a scattered pattern with varying shapes and geometries. The mathematical formula for Voronoi strut structures is given below [26] :

$$V(pi) = \left\{ \frac{p}{d(p,pi)}, \leq d(p,pj), j \neq i, i, j = 1,2, \dots, n \right\} \quad (3)$$

where $V(p_i)$ represents the 3D Voronoi polygon on seed p_i, $p_1 \ldots\ldots$ p_n are the definite seeds in 3D space, and $d(p$ and $p_i)$ is the usual Euclidean distance between p and pi. These structures are modelled by using nTopology (3.40.2). Figure 3 shows the workflow of tibial implant optimization with lattice structures. Firstly, Figure 3a shows a solid tibial implant and Figure 3b shows the region of lattice structure which will be applied on the tibial tray plate by topology optimization. As a result, the tibial tray plate contains gyroid lattice structures as shown in Figure 3c.

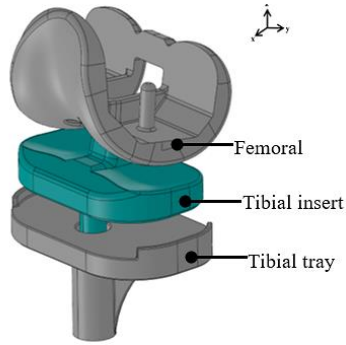

Figure 1: 3D model of total knee implant

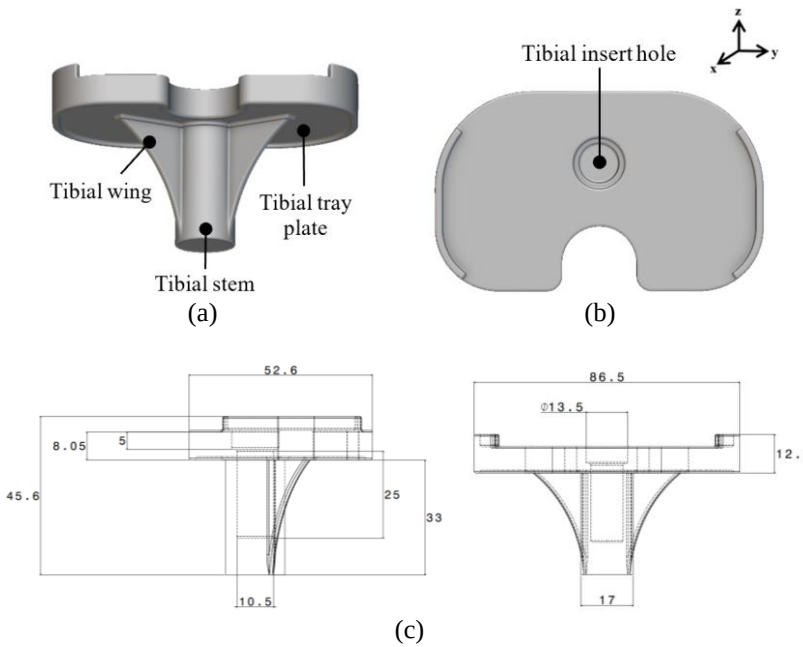

Figure 2: 3D model of tibial tray: (a) parts of tibial tray [22], (b) top view of tibial tray, and (c) geometry of tibial tray (mm)

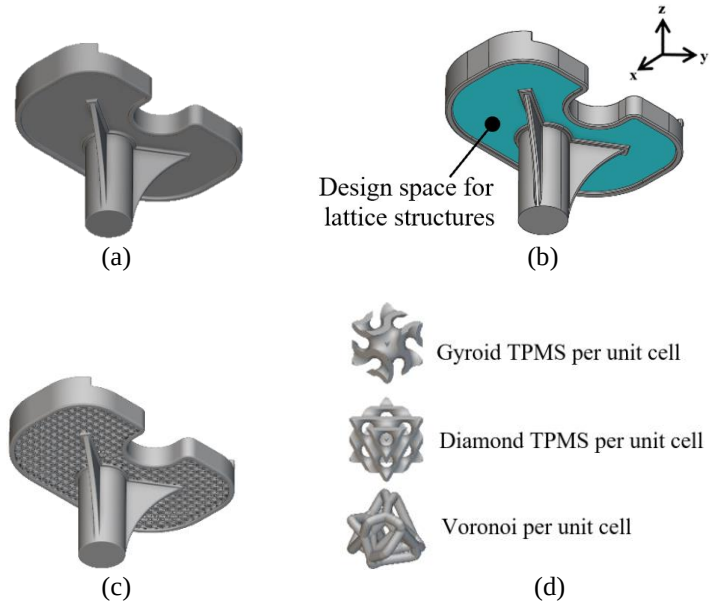

Figure 3: Workflow of tibial tray optimization: (a) solid tibial tray, (b) design region of tibial tray plate, (c) tibial tray with gyroid structures, and (d) TPMS and Voronoi structure per unit cell

For both uniform and non-uniform lattice structures, the size unit cell is 3 mm in order to maintain 50% of relative density. On the tibial tray plate, for uniform lattice structure, and diamond had a constant sheet thickness of 480 µm, meanwhile gyroid and Voronoi had a constant sheet thickness of 580 µm. As for the non-uniform lattice structure, the tibial tray plate had various ranges of sheet thickness. The non-uniform lattice for the gyroid structure had a functionally graded sheet thickness of 520-1150 µm and the diamond structure had a functionally graded sheet thickness of 440-710 µm. Moreover, for Voronoi lattice structure the functionally graded sheet thickness is between 540-850 µm. The porosity Ø of the lattice structure for both and non-uniform lattice structure is 50% determined by Equation 4. According to Arabnejad et al. [27], to ensure effective osseointegration the porosity had to be at a minimum value of 50%.

$$\text{Porosity } \emptyset = 1 - \frac{\text{Volume of scaffold}}{\text{Volume of solid structure}} \quad (4)$$

Finite Element Analysis (FEA)

The FEA is used on the tibial tray to resolve stress that occurs under various loading conditions of the optimized tibial tray. The tibial tray is meshed with

four nodes of quadratic tetrahedral elements (C3D10) of size 1.1 mm size as depicted in Figure 4. The convergence analysis is performed as shown in Figure 5 to determine the optimum number of element sizes for each design tibial tray, where the number of elements of solid tibial tray is 736, 326 and the number of nodes element is 1.12 million.

Figure 4: Mesh of solid tibial tray

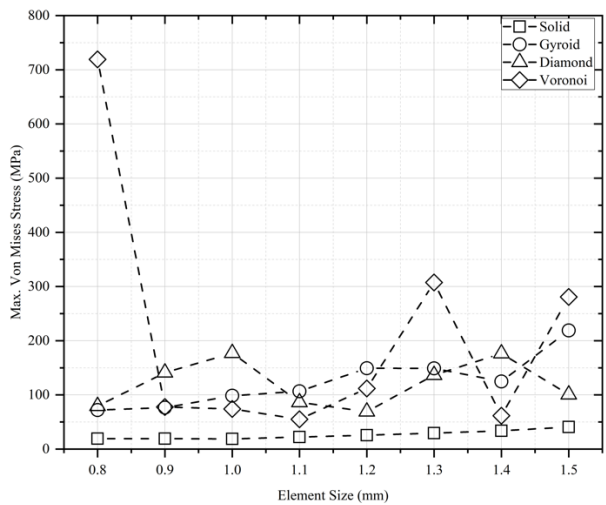

Figure 5: Convergence graph of the tibial tray for solid and variation lattice structures

The boundary conditions that mimic the actual knee joint mechanics are used for the simulation. In this case, the fixed support condition is applied at the bottom of the tibial stem to prevent any rotation and movement [28]. The axial loads of 3100 N are applied on the tibial surface which is based on walking movement due to the result of Bergmann et al. [29] who reported the knee loads are based on the percentage of weight shown in an average body

weight of 75 kg. Figure 6 illustrates the boundary condition setup of the tibial tray case.

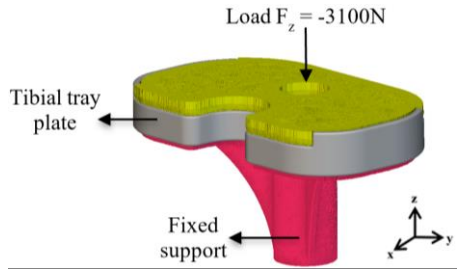

Figure 6: Boundary condition of tibial tray

The material selected for this study is titanium alloy of grade Ti6Al4V which offers good biocompatibility and corrosion resistance, besides having strength and good mechanical properties [30]. Table 1 indicates the properties of Ti6Al4V.

Table 1: Mechanical properties of Ti6Al4V [31]-[33]

Mechanical properties	Values
Density, ρ	4.43 g/cm^3
Elastic modulus, E	113.8 GPa
Poisson ratio, v	0.342
Yield strength, σ	973 MPa
Ultimate yield strength, σ_{ult}	1058 MPa

Results and Discussion

As reported in previous research, trabecular bone consists a range of 40-95% porosity [34]. For this research, the range porosity used is 50% for uniform and non-uniform lattice structures as mentioned before to enhance osseointegration [27]. Figure 7 illustrates a tibial tray with lattice structure (a, c, e) and single unit cell (b, d, f) of three different lattice structures gyroid, diamond, and Voronoi. All lattice structures are designed in 3 mm per unit cell to maintain the similarity of relative density for each structure which is 50%. In the second optimization phase, the relative density of the sheet lattice structure is controlled by the changes in wall thickness as illustrated in Figure 8. Relative density can form a huge difference even though there is the smallest change in wall thickness [35]. As an example, the unit cell for the gyroid with 3 mm has a relative density of 50% for the wall thickness of 0.58 mm, while

an increase in the wall thickness of 1.15 mm contributes to the increase in relative density of 81%. Moreover, due to the variation of lattice structures applied on the tibial tray, it shows the differences in the affected area of stress distribution as depicted in Figure 9. Meanwhile, the values of the maximum Von Mises stress of each tibial tray model are shown in Table 2. The displacement distribution of the tibial tray is shown in Figure 10 and Table 3 shows the values of the total deformation of the tibial tray.

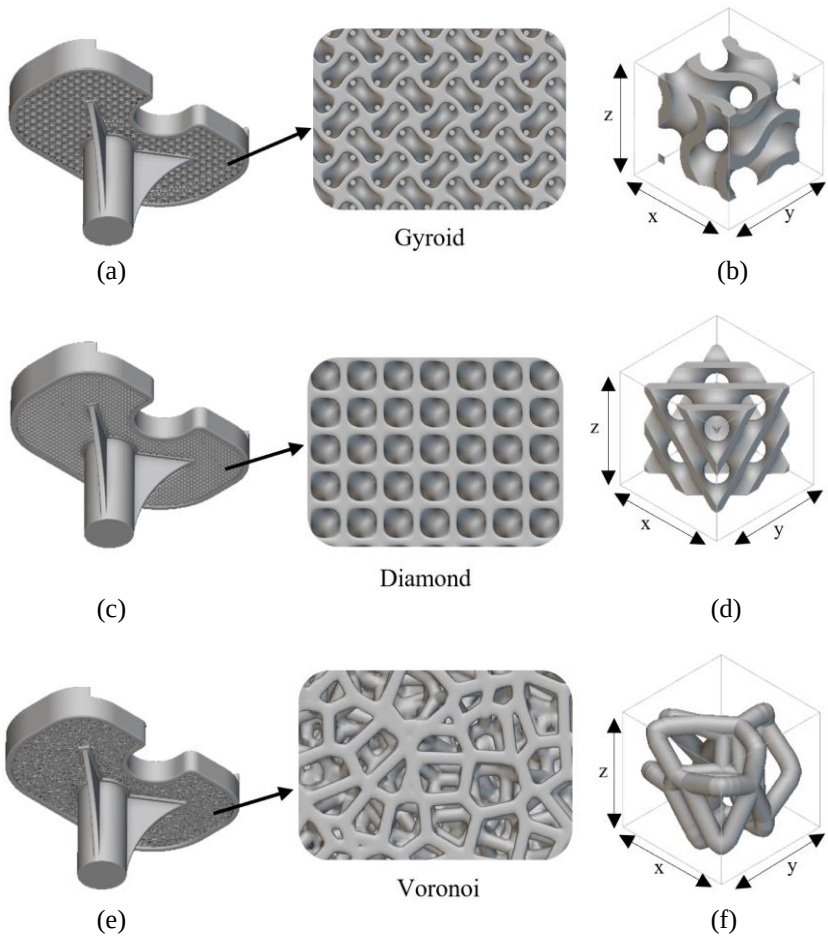

Figure 7: Gyroid structure; (a) tibial tray with lattice structure, (b) single unit cell diamond structure, (c) tibial tray with lattice structure, (d) single unit cell Voronoi structure, (e) tibial tray with lattice structure, and (f) single unit cell

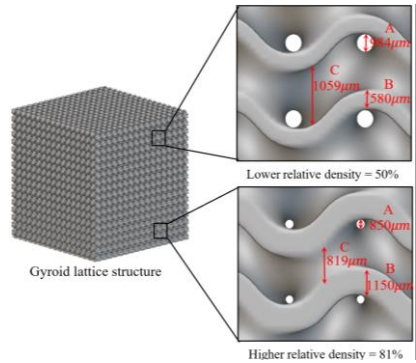

(a)

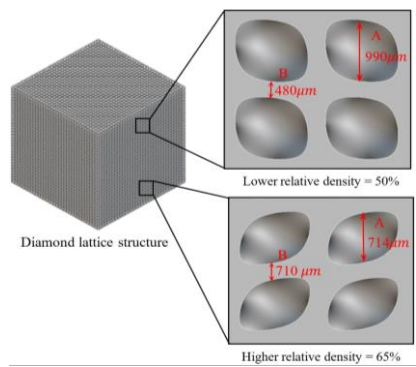

(b)

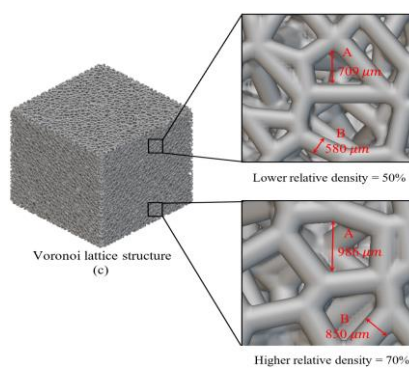

(c)

Figure 8: Relative density of various lattice structure in cube size of 50 mm; (a) pores size, (b) sheet thickness of lattice structure, and (c) length between sheet thickness

It is significant to evaluate the occurrence of solid tibial implant stress distribution area to further the topology optimization process. Since the force distribution is exerted on the tibial tray, it is shown in Figure 9a that the maximum stress distribution occurs on the edge of the tibial tray rather than the tibial stem area. Therefore, topology optimization can be reduced on the tibial tray region to reduce the stress behaviour. The maximum stress escalates up to 22.29 MPa on a specific point which does not indicate the total mechanical behaviour of the tibial implant. Furthermore, the maximum stress is in the allowable range which is below the material yield point as shown in Table 2.

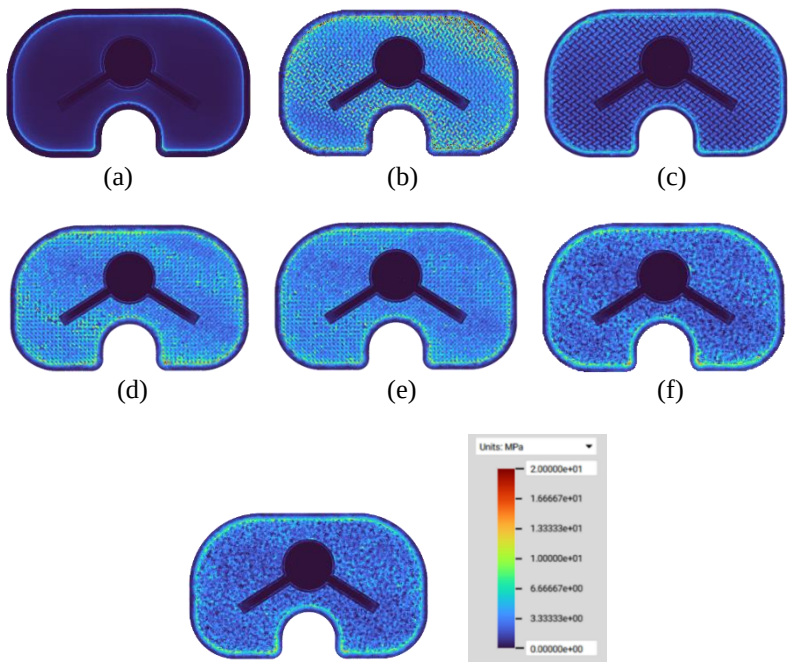

Figure 9: Stress distribution on tibial tray of solid and different lattice structures; (a) solid, (b) uniform lattice structure of gyroid, (c) non-uniform lattice structure of gyroid, (d) uniform lattice structure of diamond, (e) non-uniform lattice structure of diamond, (f) uniform lattice structure of Voronoi, and (g) non-uniform lattice structure of Voronoi

As for the Voronoi structure, high stress distribution occurs on the edge of the tibial tray. The highest strength is shown in the tibial implant which contains a Voronoi structure with a value of maximum stress of only 55 MPa due to the configuration of lattice structure being more scattered compared to

the gyroid and diamond lattice structure. In addition, the tibial implant that contains a diamond structure shows a maximum stress value of 86.36 MPa. Meanwhile, the tibial implant with a gyroid structure exhibits a maximum stress value of 161.85 MPa. The maximum stress increases in the first optimization phase because the solid area of the tibial tray is reduced through topology optimization of lattice structures which contribute to reducing the surface area of the tibial tray. Figures 9b, d, and f show the stress distribution for the first phase optimization.

Table 2: Maximum Von Mises stress of tibial tray (MPa)

Design of tibial tray	Von Mises stress (MPa)
Solid	22.29
Uniform lattice structure	
Gyroid	161.85
Diamond	86.36
Voronoi	55.0
Non-uniform lattice structure	
Gyroid	61.65
Diamond	49.74
Voronoi	35.83

All lattice structures applied on the tibial tray region are due to high stress that appears on it. In the first optimization phase, stress distribution occurs on the lattice area from the edge of the tibial implant to the center of the tibial for gyroid and diamond structures as indicated in Figure 10.

According to [36], as the lattice structures are applied to the hip implant, the value of maximum stress increases as compared to the maximum stress of the solid component. However, in order to achieve an allowable value of maximum stress, further optimization is needed to be performed by varying the range of relative density of lattice structure by a functionally graded lattice structure. It shows similarities to this research, the maximum stress of the tibial tray is increased as the lattice structures are applied on the tibial tray region. In comparison to this research, the maximum stress of the first optimization phase is still under the allowable material yield point which is 973 MPa. However, further optimization needs to be done to achieve comparable maximum stress to solid tibial implants and enhance the mechanical performance of tibial implants. Furthermore, there are studies that showed the combination of solid and lattice structures has improved the mechanical performance of tibial implants [37].

The second optimization phase continues with functionally graded lattice structures. The total relative density of the tibial tray and the relative density lattice structure region remain constant. For TPMS-based lattice, a sheet network offers good mechanical properties due to a high surface area to

volume ratio [38]. On the other hand, the Voronoi structure changes in terms of strut thickness. High stress region on the tibial tray is required to increase wall thickness compared to low stress region. The differences of stress distribution of the first optimization in Figures 9b, d, and f are compared to the second optimization in Figures 9c, e, and g which showed a reduction in the affected region of lattice structure. Figure 10 shows a close-up of stress distribution reduced from the first optimization compared to the second optimization. The percentage of maximum stress for gyroid structure reduces by about 61.91% from the first optimization to the second optimization while diamond structure reduces by 42.40% and Voronoi structure decreases by 34.85%. This demonstrates that the non-uniform lattice structure is adequate to withstand the same load exerted on the tibial tray in the first optimization with lower maximum stress. Moreover, as the wall thickness in lattice structures increases, it contributes to reducing maximum stress on each structure. This is due to the increasing surface area of lattice structures on the force exerted area of the tibial tray. According to Zineddine et al. [39], the beam thickness of lattice structures affects the amount of maximum stress by assuming the increase of cross-sectional surface of beam structures. Even though this research uses a triply periodic minimal surface (gyroid and diamond) and Voronoi lattice structure, the similar concept of force that affects the surface area is comparable.

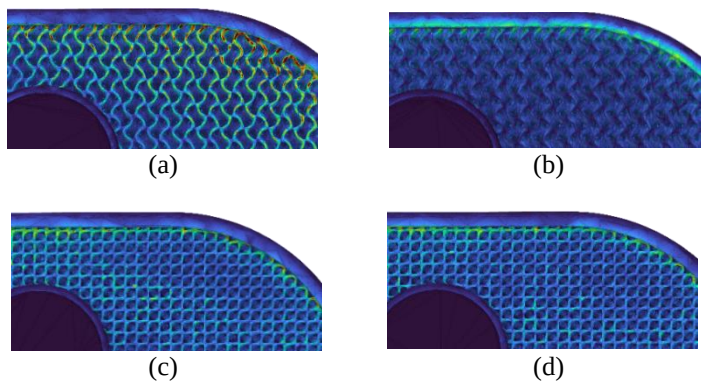

Figure 10: Stress distribution of; (a) uniform gyroid lattice structures, (b) non-uniform gyroid lattice structures, (c) uniform diamond lattice structures, and (d) non-uniform lattice structures

In addition, the deformation result shows that the highest deformation among the tibial tray model is the Voronoi structure in uniform lattice structure with the value of 0.000497 mm. Meanwhile, the lowest deformation is 0.000278 mm for non-uniform structure of the diamond. Figure 11 shows the

deformation distribution of varies types of lattice structures for uniform and non-unifrom sturctures.

Table 3: Total displacement of tibial tray (mm)

Design of tibial tray	Maximum displacement (mm)
Solid	0.000294
Uniform lattice structure	
Gyroid	0.000339
Diamond	0.000291
Voronoi	0.000497
Non-uniform structure	
Gyroid	0.000290
Diamond	0.000278
Voronoi	0.000459

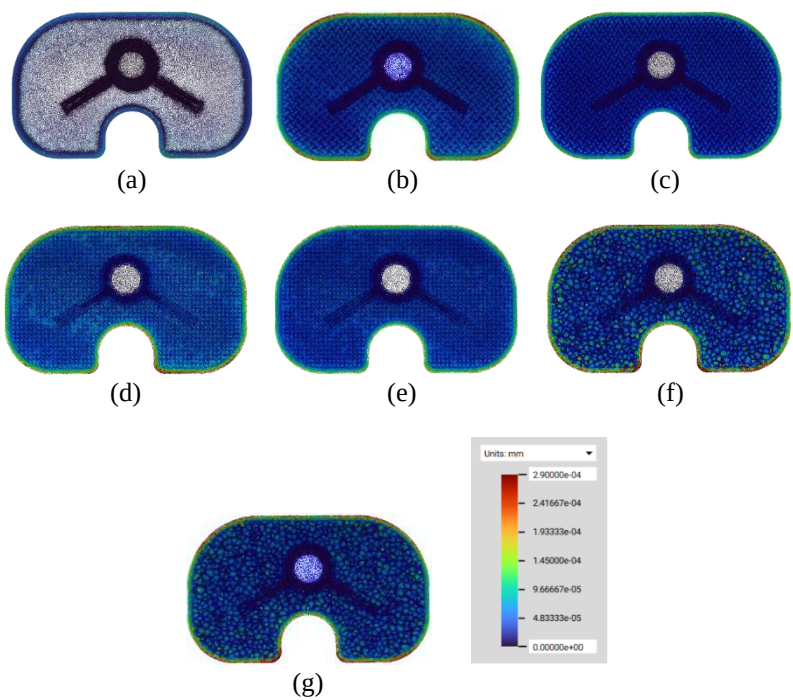

Figure 11: Displacement distribution on tibial tray of solid and different lattice structures: (a) solid, (b) uniform lattice structure of gyroid, (c) non-uniform lattice structure of gyroid, (d) uniform lattice structure of diamond, (e) non-uniform lattice structure of diamond, (f) uniform lattice structure of Voronoi, and (g) non-uniform lattice structure of Voronoi

All structures demonstrate a decrease deformation distribution for non-uniform structures as the lattice structure consists of a variation of wall thickness. Furthermore, all deformations occur at the top of the tibial tray region for all types of lattice structures and solids as demonstrated in Figure 10. The distribution of force exerted on the top of the tibial region causes maximum displacement to occur on the top of the tibial region compared to the tibial wing and stem region.

However, this research had several limitations. The tibial implant with different types of lattice structures (gyroid, diamond, and Voronoi) was simulated only by static conditions. In order to obtain acceptable data for the optimization, further studies need to be done as the walking conditions require dynamic motions. According to the literature review, the main parameters used in this research are different types of lattice structure and relative density of lattice structure which showed a significant effect on the maximum stress distribution of tibial implant. However, the effect of porosity was not mentioned in this study; thus, it should be considered as it is widely used in previous literature reviews.

Conclusion

In the present study, topology optimization of three different lattices was proposed on the tibial tray to show better mechanical performance. The topology optimization applied different lattice structures such as gyroid, diamond, and Voronoi which are considered to have superior mechanical performance. A lattice structure was applied on high-stress region to maintain the optimal mass of the tibial tray. Moreover, the optimization of the lattice structure was continued by functional gradation. By this continuity of optimization, various ranges of sheet thickness of lattice structure contributed to enhancing mechanical behaviour while the stress distribution for all lattice structures remained within the allowable range. Above all, it was examined that the tibial tray consisting of Voronoi structures showed the best mechanical behaviour compared to gyroid and diamond for both phases of lattice optimization. By topology optimization, the weight reduction of optimized tibial reached up to 40% compared to solid tibial meanwhile the density was reduced by about 48%. As for future work, the fabrication of a tibial implant by using selective laser melting and the evaluation of mechanical behaviour should be measured and compared between simulation and experimental values.

Contributions of Authors

Concept: Mohd Shahriman Adenan; Methodology: Nurasyrani Rabuan, Yupiter HP Manurung, Mohd Shahriman Adenan; Results and Discussion: Nurasyrani Rabuan, Mohd Afzan Mohd Anuar, Solehuddin Shuib, Yupiter HP Manurung, Mohd Shahriman Adenan; Review and Editing: Nurasyrani Rabuan, Mohd Shahriman Adenan. All authors have agreed to the publication of the manuscript.

Funding

This work received funding from Universiti Teknologi MARA with grant code 600-RMC/KEPU 5/3 (009/2021) Study of Design for Additive Manufacturing (DFAM) for Coated Hip Implant for the 3D printing process of the TKA implants

Conflict of Interests

One of the authors, Mohd Afzan Mohd Anuar, is an assistant managing editor of the Journal of Mechanical Engineering (JMechE). The author has no other conflict of interest to note.

Acknowledgment

The authors express the highest gratitude towards nTop. (USA) for the software license and never-ending support in the simulation section.

References

[1] M. Nematollahi, A. Jahadakbar, M. J. Mahtabi, and M. Elahinia, Additive manufacturing (AM), 2nd Ed. Elsevier Ltd., 2019. doi: 10.1016/B978-0-08-102666-3.00012-2.

[2] J. Ni, H. Ling, S. Zhang, Z. Wang, Z. Peng, C. Benyshek, R. Zan, A.K. Miri, Z. Li, X. Zhang, J. Lee, K.-J. Lee, H.-J. Kim, P. Tebon, T. Hoffman, M.R. Dokmeci, N. Ashammakhi, X.Li, and A.Khademhosseini, "Three-dimensional printing of metals for biomedical applications," *Materials Today Bio*, vol. 3, 2019. doi: 10.1016/j.mtbio.2019.100024.

[3] A. R. Balwan and V. D. Shinde, "Development of patient specific knee joint implant," *Materials Today Proceedings*, vol. 27, no. 1, pp. 288–293,

2019. doi: 10.1016/j.matpr.2019.11.032.

[4] X. Wang, S. Xu, S. Zhou, W.Xu, M.Leary, P.Choong, M.Qian, M.Brandt, Y.M.Xie, "Topological design and additive manufacturing of porous metals for bone scaffolds and orthopaedic implants: A review," *Biomaterials*, vol. 83, pp. 127–141, 2016. doi: 10.1016/j.biomaterials.2016.01.012.

[5] J. P. Luo, Y.J.Huang, J.Y.Xu, J.F.Sun, M.S. dargush, C.H.Hou, L.Ren, R.Z.Wang, T.Ebel, and M.Yan, "Additively manufactured biomedical Ti-Nb-Ta-Zr lattices with tunable Young's modulus: Mechanical property, biocompatibility, and proteomics analysis," *Materials Science and Engineering: C*, vol. 114, p. 110903, 2020.

[6] J. J. Callaghan, D. E. DeMik, N. A. Bedard, A. N. Odland, W. M. Kane, and S. M. Kurtz, "Tibial tray fracture in a modern prosthesis with retrieval analysis," *Arthroplasty Today*, vol. 4, no. 2, pp. 143–147, 2018. doi: 10.1016/j.artd.2017.12.005.

[7] F. Galloway, M. Kahnt, H. Ramm, P. Worsley, S. Zachow, P.Nair, and M.Taylor,"A large scale finite element study of a cementless osseointegrated tibial tray," *Journal of Biomechanics*, vol. 46, no. 11, pp. 1900–1906, 2013. doi: 10.1016/j.jbiomech.2013.04.021.

[8] M. Peto, "Topology and lattice-based structural design optimization for additively manufactured medical implants," Thesis, Denton, Texas, p. 55, 2019.

[9] Z. Guoqing, Y. Yongqiang, L. Hui, S. Changhui, X. Ran, and Y. Jiakuo, "Modeling and manufacturing technology for personalized biological fixed implants," *Journal of Medical and Biological Engineering*, vol. 37, no. 2, pp. 191–200, 2017. doi: 10.1007/s40846-016-0215-z.

[10] J. Zhang, Y. Shen, Y. Sun, J. Yang, Y. Gong, K. Wang, Z.Zhang, X. Chen and L. Bai, "Design and mechanical testing of porous lattice structure with independent adjustment of pore size and porosity for bone implant," *Journal of Materials Research and Technology*, vol. 18, pp. 3240–3255, 2022. doi: 10.1016/j.jmrt.2022.04.002.

[11] H. Zhou, M. Zhao, Z. Ma, D. Z. Zhang, and G. Fu, "Sheet and network based functionally graded lattice structures manufactured by selective laser melting: Design, mechanical properties, and simulation," *International Journal of Mechanical Sciences*, vol. 175, p. 105480, 2020. doi: 10.1016/j.ijmecsci.2020.105480.

[12] L. Yang, C. Yan, C. Han, P. Chen, S. Yang, and Y. Shi, "Mechanical response of a triply periodic minimal surface cellular structures manufactured by selective laser melting," *International Journal of Mechanical Sciences*, vol. 148, pp. 149–157, 2018. doi: 10.1016/j.ijmecsci.2018.08.039.

[13] C. Yan, L. Hao, A. Hussein, and P. Young, "Ti-6Al-4V triply periodic minimal surface structures for bone implants fabricated via selective laser melting," *Journal of The Mechanical Behavior of Biomedical Materials*,

vol. 51, pp. 61–73, 2015. doi: 10.1016/j.jmbbm.2015.06.024.
[14] L. Dall'Ava, H. Hothi, A. Di Laura, J. Henckel, and A. Hart, "3D printed acetabular cups for total hip arthroplasty: A review article," *Metals (Basel)*, vol. 9, no. 7, 2019. doi: 10.3390/met9070729.
[15] S. Limmahakhun, A. Oloyede, N. Chantarapanich, P. Jiamwatthanachai, K. Sitthiseripratip, Y. Xiao, and C. Yan, "Alternative designs of load−sharing cobalt chromium graded femoral stems," *Materials Today Communications*, vol. 12, pp. 1–10, 2017. doi: 10.1016/j.mtcomm.2017.05.002.
[16] O. Al-Ketan and R. K. Abu Al-Rub, "Multifunctional mechanical metamaterials based on triply periodic minimal surface lattices," *Advanced Engineering Materials*, vol. 21, no. 10, 2019. doi: 10.1002/adem.201900524.
[17] G. Wang, L. Shen, J. Zhao, H. Liang, D.Xie, Z. Tian, and C. Wang "Design and compressive behavior of controllable irregular porous scaffolds: based on voronoi-tessellation and for additive manufacturing," *ACS Biomaterials Science & Engineering*, vol. 4, no. 2, pp. 719–727, 2018. doi: 10.1021/acsbiomaterials.7b00916.
[18] H. Liang, Y. Yang, D. Xie, L. Li, N. Mao, C. Wang, Z, Tian, Q. Jiang, and L.Shen, "Trabecular-like Ti-6Al-4V scaffolds for orthopedic: fabrication by selective laser melting and in vitro biocompatibility," *Journal of Materials Science & Technology*, vol. 35, no. 7, pp. 1284–1297, 2019. doi: 10.1016/j.jmst.2019.01.012.
[19] M. Benedetti, J. Klarin, F. Johansson, V. Fontanari, V. Luchin, G.Zappini, and A. Molinari, "Study of the compression behaviour of Ti6Al4V trabecular structures produced by additive laser manufacturing," *Materials (Basel)*, vol. 12, no. 9, 2019. doi: 10.3390/ma12091471.
[20] S. Shuib, M. A. Azemi, I. Binti, M. Arrif, and N. S. Hamizan, "Design for additive manufacturing and finite element analysis for high flexion total knee replacement (TKR)," *Journal of Mechanical Engineering*, vol. 18, no. 2, pp. 97–110, 2021.
[21] N. Jindal, S. S. Sankhala, and V. Bachhal, "The role of fusion in the management of burst fractures of the thoracolumbar spine treated by short segment pedicle screw fixation: A prospective randomised trial," *The Journal of Bone and Joint Surgery British Volume*, vol. 94 B, no. 8, pp. 1101–1106, 2012. doi: 10.1302/0301-620X.94B8.
[22] G. Zhang, J. Li, X. Zhou, Y. Zhou, and A. Wang, "Optimal design and processing technology of 3D printed tibial implants," *Coatings*, vol. 12, no. 5, p. 561, 2022. doi: 10.3390/coatings12050561.
[23] C. Pan, Y. Han, and J. Lu, "Design and optimization of lattice structures: A review," *Applied Sciences*, vol. 10, no. 18, pp. 1–36, 2020. doi: 10.3390/APP10186374.
[24] T. Maconachie, M. Leary, B. Lozanovski, X. Zhang, M. Qian, O.

Faruque, and M. Brandt, "SLM lattice structures: Properties, performance, applications and challenges," *Materials and Design*, vol. 183, p. 108137, 2019. doi: 10.1016/j.matdes.2019.108137.

[25] C. Chatzigeorgiou, B. Piotrowski, Y. Chemisky, P. Laheurte, and F. Meraghni, "Numerical investigation of the effective mechanical properties and local stress distributions of TPMS-based and strut-based lattices for biomedical applications," *Journal of The Mechanical Behavior of Biomedical Materials*, vol. 126, Feb. 2022. doi: 10.1016/j.jmbbm.2021.105025.

[26] A. Dobrin, "A Review Of Properties And Variations Of Voronoi Diagrams." Oct 31, 2023. [Online]. Available: chrome-extension://efaidnbmnnnibpcajpcglclefindmkaj/https://www.whitman.edu/documents/academics/mathematics/dobrinat.pdf (Accessed Oct 31, 2023).

[27] S. Arabnejad, R. Burnett Johnston, J. A. Pura, B. Singh, M. Tanzer, and D. Pasini, "High-strength porous biomaterials for bone replacement: A strategy to assess the interplay between cell morphology, mechanical properties, bone ingrowth and manufacturing constraints," *Acta Biomateralia*, vol. 30, pp. 345–356, 2016. doi: 10.1016/j.actbio.2015.10.048.

[28] A. Z. E. A. Arab, A. Merdji, A. Benaissa, S. Roy, B. B. Bouiadjra, K. Layadi, A. Ouddane, and O. Mukdadi, "Finite-Element analysis of a lateral femoro-tibial impact on the total knee arthroplasty," *Computer Methods and Programs in Biomedicine*, vol. 192, 2020. doi: 10.1016/j.cmpb.2020.105446.

[29] G. Bergmann, A. Bender, F. Graichen, J. Dymke, A. Rohlmann, A. Trepczynski, M. Heller, and I. Kutzner, "Standardized loads acting in knee implants," *PLoS One*, vol. 9, no. 1, p.e86035, 2014. doi: 10.1371/journal.pone.0086035.

[30] A. Deing, B. Luthringer, D. Laipple, T. Ebel, and R. Willumeit, "A porous TiAl6V4 implant material for medical application," *International Journal of Biomaterials*, vol. 2014, no. 10, p. 904230, 2014. doi: 10.1155/2014/904230.

[31] T. Majumdar, N. Eisenstein, J. E. Frith, S. C. Cox, and N. Birbilis, "Additive Manufacturing of Titanium Alloys for Orthopedic Applications: A Materials Science Viewpoint," *Advanced Engineering Materials*, vol. 20, no. 9, 2018. doi: 10.1002/adem.201800172.

[32] S. Liu and Y. C. Shin, "Additive manufacturing of Ti6Al4V alloy: A review," *Materials and Design*, vol. 164, 2019, doi: 10.1016/j.matdes.2018.107552.

[33] Renishaw, "Ti6Al4V ELI-0406 powder for additive manufacturing Process specification Powder description Titanium alloy powder," 2017. [Online]. Available: www.renishaw.com/contact

[34] K. Nelson, C. N. Kelly, and K. Gall, "Effect of stress state on the

mechanical behavior of 3D printed porous Ti6Al4V scaffolds produced by laser powder bed fusion," *Materials Science and Engineering: B*, vol. 286, p. 116013, 2022. doi: 10.1016/j.mseb.2022.116013.

[35] O. Al-Ketan, D. W. Lee, R. Rowshan, and R. K. Abu Al-Rub, "Functionally graded and multi-morphology sheet TPMS lattices: Design, manufacturing, and mechanical properties," *Journal of the Mechanical Behavior of Biomedical Materials*, vol. 102, p. 103520, 2020. doi: 10.1016/j.jmbbm.2019.103520.

[36] N. Kladovasilakis, K. Tsongas, and D. Tzetzis, "Finite element analysis of orthopedic hip implant with functionally graded bioinspired lattice structures," *Biomimetics*, vol. 5, no. 3, p. 44, 2020. doi: 10.3390/BIOMIMETICS5030044.

[37] Z. Guoqing, L. Junxin, Z. Chengguang, X. Juanjuan, Z. Xiaoyu, and W. Anmin, "Design Optimization and Manufacturing of Bio-fixed tibial implants using 3D printing technology," *Journal of the Mechanical Behavior of Biomedical Material*, vol. 117, p. 104415, 2021. doi: 10.1016/j.jmbbm.2021.104415.

[38] O. Al-Ketan, R. Rezgui, R. Rowshan, H. Du, N. X. Fang, and R. K. Abu Al-Rub, "Microarchitected Stretching-Dominated Mechanical Metamaterials with Minimal Surface Topologies," *Advanced Engineering Materials*, vol. 20, no. 9, p. 1800029, 2018.

[39] Z. Izri, A. Bijanzad, S. Torabnia, and I. Lazoglu, "In silico evaluation of lattice designs for additively manufactured total hip implants," *Computers in Biology and Medicine*, vol. 144, p. 105353, 2022. doi: 10.1016/j.compbiomed.2022.105353.